Modelling and applications of dissolution of rocks in geoengineering

Farid Laouafa, Jianwei Guo, Michel Quintard

Modelling and applications of dissolution of rocks in geoengineering

Farid Laouafa[1,*], Jianwei Guo[2], Michel Quintard[3]

[1]National Institute for Industrial Environment and Risks (INERIS), Verneuil en Halatte, France.

[2]School of Mechanics and Aerospace Engineering, Southwest Jiaotong University, 610031 Chengdu, China

[3]Université de Toulouse ; INPT, UPS ; IMFT (Institut de Mécanique des Fluides de Toulouse) ; Allée Camille Soula, F-31400 Toulouse, France and CNRS; IMFT; F-31400 Toulouse, France

[*]corresponding authors: farid.laouafa@ineris.fr

Summary

The subsoil contains many evaporites such as limestone, gypsum or salt. Such rocks are very sensitive to water. The deposit of evaporites raises questions of their dissolution with time and the mechanical-geotechnical impact on the neighboring zone. Depending on the configuration of the site and the location of the rocks, the dissolution can lead to surface subsidence, the formation of sinkholes and landslides for instance. In this article, we present an approach that describes the dissolution process and the coupling with geotechnical engineering. In the first part we set the physico-mathematical framework, the hypothesis, and the limitations in which the dissolution process is stated. The physical interface between the fluid and the rock (porous solid) is represented by a diffuse interface of finite thickness. We briefly describe, in the framework of porous media, the step needed to upscale the microscopic scale (pore scale) model to macroscopic scale (Darcy scale). Although the constructed method has a rather large range of application, we will restrict the application to saline and gypsums rocks. The second part is mainly devoted to the geotechnical consequences of the dissolution of gypsum material. We then analyze the effect of dissolution in the vicinity of a soil dam or slope and the partial dissolution of a gypsum pillar by a thin layer of water. These theoretical examples show the relevance and the potential of the approach in the general framework of geoengineering problems.

Key words: dissolution, modelling, scaling, evaporite, deformation, plasticity

1. Introduction

Natural or human induced dissolution of soluble of soluble rocks in contact with water affects many soils and subsoils. These perturbations result in a redistribution of the effective or total stress field and thus the deformation of the soil and subsoil. The mechanical response of the soil and its impact on the surface depends on the location and the geometric features of the cavities resulting from dissolution. This damage is mainly related to the “change of phase”,

from solid to liquid, of part of the domain. With this change the stress field can reach critical states but also plasticity or failure in part of the domain in question. Examples of potential effects include subsidence, sinkholes, impacts on geo-structures, etc. (James et al. 1978, Castellanza et al. 2008, Waltham et al. 2005, Bell et al. 2000, Gerolymatou et al. 2008 Swift and Reddish 2002). Particular attention must be paid to the understanding and control of this phenomenon, which is very important in geoengineering contexts.

An intrinsic difficulty in the dissolution of underground rocks is the time dependency of the geotechnical problem, but there lacks the in-situ data concerning of their space and time evolution. Rock dissolution occurs as long as the fluid flow in the subsurface is under-saturated. In this article we will concentrate mainly on the dissolution of gypsum rocks ($CaSO_4.2H_2O$), even though the numerical approach implemented to describe dissolution has a broader scope. Therefore, we also include reference to some problems involving salt (NaCl). A substantial contrast between a problem involving salt and e that involving gypsum is their solubility and the corresponding physical instabilities. Let us note, that the solubility, defined as the maximum amount of a chemical species that dissolves in a specified amount of solvent (water) at a prescribed temperature, of evaporites can range from several orders of magnitude. For example, the solubilities of salt, gypsum, and limestone are 360, 2.50, and 0.013 g/l, respectively (Freeze et al. 1974).

Answering the questions posed by the dissolution process is a difficult and non-trivial exercise. Indeed, the problem exhibits several multi-scale and multi-physical features, couplings and non-linearities. One difficulty is related to the precision required in the description and quantification of the recession rate of the solid-liquid interface at the macroscopic scale. To circumvent this scientific drawback, a specific mathematics statement of the physico-chemical and transport equations at the microscopic or pore scale is established. Another difficulty is to tackle dissolution phenomena at in-situ or, geo-structures scales. Let underline that such problems are linked to the strong physical coupling with other processes, such as the mechanical behavior of rocks. In contrast to the phenomenological or "averaged" approaches of the dissolution process (Jeschke et al., 2001; Jeschke and Dreybrodt, 2002), our approach begins at the microscopic scale.

In this paper we briefly present the approach proposed in order to model and solve the dissolution problem. The method is built on strong theoretical bases but also supported by numerical modelling. The mathematical formalization of the problem of the dissolution surface and its kinetics is initially built at the pore scale. A possible candidate numerical

approach to describe dissolution is a method that explicitly follows during the process the fluid-solid interface In this case, the ALE (Arbitrary Lagrangian-Eulerian) method proposed by Donea (Donea et al. 1982) is well suited. An alternative approach no longer views the interface as a sharp and discontinuous boundary between solid and liquid, but considers the interface having a finite thickness and well-defined properties (notably continuity), in other term a diffuse interface (Anderson et al., 1998, Collins et al., 1985). We limit our development to two-phase porous media and we suppose fluid saturated porous rocks.

We present the physical and mathematical basis of the pore scale dissolution model and the upscaled Diffuse Interface Model (DIM) using a volume-averaged theory. The part of this article that dedicated to the geomechanical consequences considers only gypsum rocks. Whatever the hydrogeological configuration, the dissolution of gypsum (lenses, pillars, etc.) in the ground raises questions in terms of geomechanical consequences: subsidence, sinkholes, stability of pillars or cavities, etc. (Gysel (2002), Toulemont (1987, 1981), Cooper (1988), Bell et al (year). The aim of the last section of this paper is to show on several 2D and 3D theoretical examples, the robustness and the potentialities of the proposed numerical dissolution approach.

The geotechnical problems to be addressed are elastoplastic. The elastoplastic constitutive model used to describe the behavior of soil and gypsum are relatively simple. The aim is not to develop a precise study of a real case but to provide an illustration of the ability of the proposed approach. This last one is valid regardless of the complexity of the constitutive model used. We will illustrate these issues in the case of plasticity within a soil mass in the vicinity of a dike and in the case of partial dissolution of an elastoplastic pillar. In all the studied configurations, the soluble gypsum is located inside porous domains.

We can see from the numerical modelling that the proposed approach has a predictive aspect. Indeed, the mechanical and dissolution coupling allows us to model the time evolution of all the fields (stresses, strains, displacements, …) and to determine the critical time beyond which severe risks can appear.

2. Mathematical formulation of the dissolution

This section is devoted to a brief review of the underlying principles of the method used for modeling the dissolution. The reader can find more detailed information on the scientific background in (Luo et al., 2012, 2014, 2015, Guo et al. 2015, 2016). At the pore scale, the dissolution problem can be posed using the classical balance equations initial and boundary

conditions. In order to achieve the expression of the "macro" DIM model, we start with these "small scale" equations to generate Darcy-scale equations, the corresponding Darcy-scale quantities and effective coefficients, using volume-averaging theory (Whitaker, 1999). After introducing the original model (micro-pore scale) for the dissolution problem, we present the upscaling method leading to the "Darcy-scale" equations. We provide a quick review of the main ideas and principles on the upscaling the pore scale equations to a macroscopic scale. The Darcy scale model that is derived from this upscaling is the one that is used for large-scale dissolution modeling.

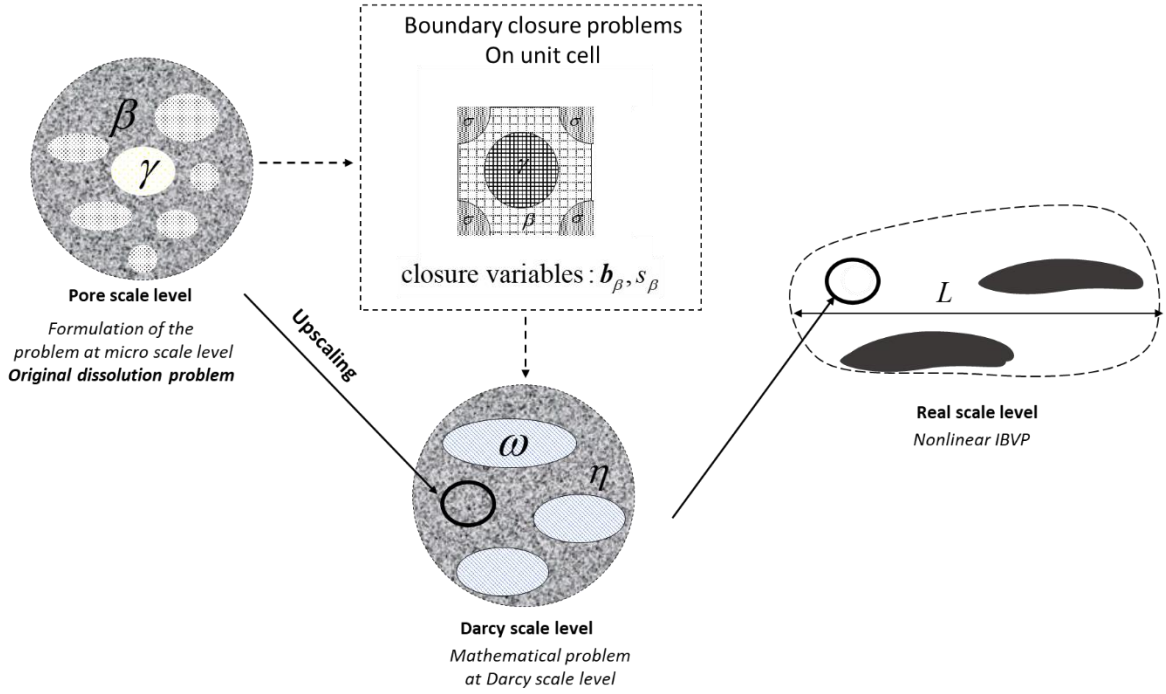

Figure 1. Sketch of the passage from microscopic to real in-situ scales, closure variables and 2D unit cell. The general notation $\beta, \gamma, \omega, \sigma, \ldots$ indicates phases (fluid, soluble phase, heterogeneities, non-soluble phase…)

The passage of the description of the phenomena from the microscopic to the real "geotechnical" scale is depicted in Fig. 1.

Before going further, note that we restrict our discussion to porous media composed of two phases, a solid porous phase and a liquid phase. The porous medium is fully saturated with liquid. More general approaches can be found in (Luo et al., 2012, 2014). To distinguish

the phases, we will use the subscript "s" to indicate the solid phase and the subscript "*l*" to indicate the liquid phase.

The so called "original dissolution problem" includes a solid/liquid sharp interface as depicted in Fig. 2. At this interface the fluid concentration $C(\overline{x},t)$ ($\overline{x}$ belongs to interface) is equal to the evaporite or equilibrium concentration C_{eq}. A key feature of the DIM method is the introduction of a phase indicator defined over the entire domain (solid and liquid). In our approach we use the porosity $\varepsilon(x,t)$ that describe the state and evolution of the dissolution. In the sharp or original problem, $\varepsilon(x,t)$ is discontinuous at the solid-liquid interface (Fig. 2). Solving the mathematical problem with this condition requires special front tracking, front marching numerical techniques (Mital et al. 2005, Tryggvason et al. 2001, Feng et al. 1994). These methods are CPU-time consuming and face numerical difficulties, in case of non-smooth geometries. With the DIM method we can be circumvented such difficulties because we do not tackle explicitly the interface space and time evolution. The partial differential equations are written instead for a continuous scalar variables, such as the porosity $\varepsilon(x,t)$ and the mass fraction $\omega_{Al}(x,t)$ (mass fraction of species *A* in the *l*-phase), which leads to a diffuse interface description as illustrated in Fig. 2.

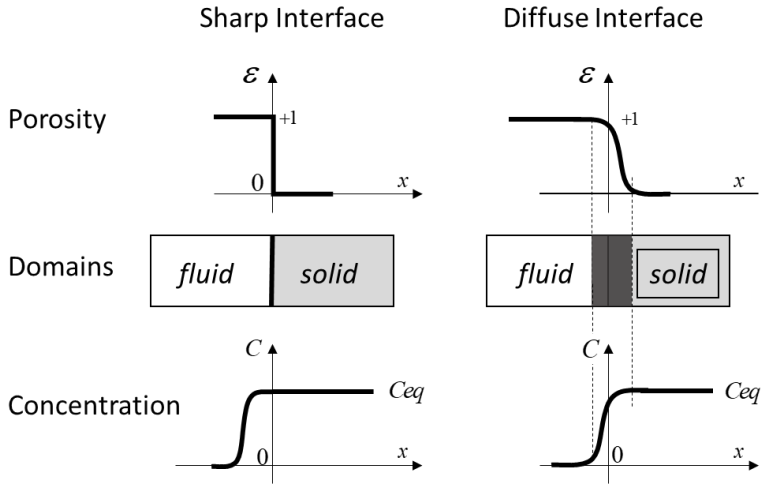

Figure 2. Porosity and concentration space-evolution when crossing sharp and a diffuse interfaces.

2.1. Pore scale model

Let us consider a binary liquid phase (l) containing chemical species *A* and *B*, and a solid phase (s) containing only chemical species *A*, as depicted in Fig. 3 (right).

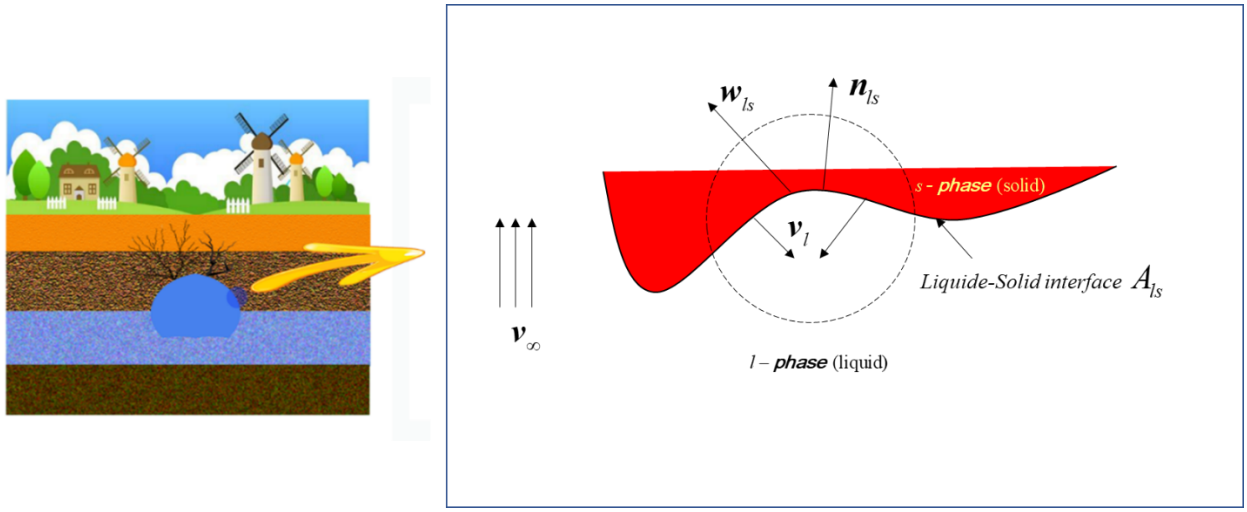

Figure 3: Sketch of in-situ cavity and focus near rock-solid/fluid interface

Let write the mass balance for two phases and the chemical species *A*. Let underline that all variables are time dependent. For the sake of readability, we simplify the notations such as for example: $\rho_l \equiv \rho_l(\boldsymbol{x},t,...)$.

$$\frac{\partial \rho_l}{\partial t} + \nabla \cdot \left(\rho_l \boldsymbol{v}_l\right) = 0 \tag{1}$$

$$\frac{\partial \rho_s}{\partial t} + \nabla \cdot \left(\rho_s \boldsymbol{v}_s\right) = 0 \tag{2}$$

$$\frac{\partial \left(\rho_l \omega_{Al}\right)}{\partial t} + \nabla \cdot \left(\rho_l \omega_{Al} \boldsymbol{v}_l\right) = \nabla \cdot \left(\rho_l \boldsymbol{D}_{Al} \nabla \omega_{Al}\right) \tag{3}$$

Here, ρ_l, ρ_s, $\boldsymbol{v}_l$, $\boldsymbol{v}_s$, ω_{Al} and $\boldsymbol{D}_{Al}$ are the density of *l*-phase, density of *s*-phase, the *l*-phase velocity, the *s*-phase velocity, the mass fraction of species *A* in the liquid and the diffusion tensor respectively.

In the following analysis, the *s*-phase is supposed immobile ($\boldsymbol{v}_s = 0$). The momentum balance for the fluid follows Navier-Stokes equations

$$\rho_l \left(\frac{\partial \boldsymbol{v}_l}{\partial t} + \boldsymbol{v}_l \cdot \nabla \boldsymbol{v}_l \right) = -\nabla P_l + \rho_l \, \mathbf{g} + \mu_l \, \nabla^2 \boldsymbol{v}_l \tag{4}$$

where P_l represents the water pressure in the *l*-phase, μ_l the liquid dynamic viscosity and $\mathbf{g}$ the gravity vector. Under some assumption (Luo et al. 2012) we have at the fluid/solid interface A_{ls}, the classical equilibrium condition, i.e.,

$$\omega_{Al} = \omega_{eq} \qquad \text{at} \qquad A_{ls} \tag{5}$$

The boundary conditions for the mass balance at the solid-liquid interface with normal outward vector $\mathbf{n}_{ls}$ can be written as follows (Fig. 3):

$$\boldsymbol{n}_{ls} \cdot \left(\rho_l \omega_{Al} \left(\boldsymbol{v}_l - \boldsymbol{w}_{ls} \right) - \rho_l \boldsymbol{D}_{Al} \nabla \omega_{Al} \right) = \boldsymbol{n}_{ls} \cdot \left(-\rho_s \boldsymbol{w}_{ls} \right) \quad \text{at } A_{ls} \tag{6}$$

where, $\boldsymbol{w}_{ls}$ is the interface velocity also called recession velocity. This equation may be used to compute explicitly the interface velocity in the ALE method for instance and can be expressed as follows:

$$\boldsymbol{n}_{ls} \cdot \boldsymbol{w}_{ls} = \frac{\rho_l}{\rho_s} \frac{1}{(1-\omega_{Al})} D_{Al} \; \boldsymbol{n}_{ls} \cdot \nabla \omega_{Al} \tag{7}$$

2.2. Upscaled macro-scale non-equilibrium model

A DIM model can be written in an appropriate way in the framework of porous medium theory. In this subsection, we describe the macroscopic Darcy-scale equations obtained by upscaling the above set of pore scale equations, using the volume averaging theory (Quintard and Whitaker, 1994, Whitaker, 1999). The reader will find in paper (Guo et al., 2016) the details of this change of scale. The representative elementary volumes (Bachmat and Bear, 1987) is illustrated in Fig. 4. We define the intrinsic average of the mass fraction Ω_{Al} and the superficial average of the velocity $\boldsymbol{V}_l$ as

$$\Omega_{Al} = \left\langle \omega_{Al} \right\rangle^l = \varepsilon_l^{-1} \left\langle \omega_{Al} \right\rangle = \frac{1}{\mathrm{V}_l} \int_{\mathrm{V}_l} \omega_{Al} \left(\boldsymbol{r} \right) d\mathrm{V} \text{ and } \boldsymbol{V}_l = \left\langle \boldsymbol{v}_l \right\rangle = \varepsilon_l \left\langle \boldsymbol{v}_l \right\rangle^l = \frac{1}{\mathrm{V}} \int_{\mathrm{V}l} \boldsymbol{v}_l \left(\boldsymbol{r} \right) d\mathrm{V} \tag{8}$$

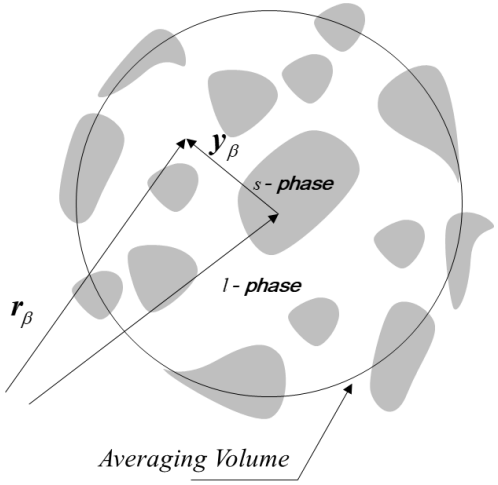

Figure 4. Averaging volume at pore scale level

After transformation the averaged form of balance equation of species *A* can be expressed as

$$\underbrace{\frac{\partial\langle\rho_l\omega_{Al}\rangle}{\partial t}}_{(a)}+\underbrace{\nabla\cdot\langle\rho_l\omega_{Al}\boldsymbol{v}_l\rangle}_{(b)}=\underbrace{\nabla\cdot\langle\rho_l\boldsymbol{D}_{Al}\nabla\omega_{Al}\rangle}_{(c)}\underbrace{-\frac{1}{\mathrm{V}}\int_{A_{ls}}\boldsymbol{n}_{ls}\cdot\rho_l\omega_{Al}\left(\boldsymbol{v}_{Al}-\boldsymbol{w}\right)dA}_{(d)} \tag{9}$$

With (a), (b), (c), (d), the accumulation, the convection, the diffusion and (d) the phase exchange terms, respectively. With several assumptions and some mathematics manipulations of the various equations, we derive the followings equations for the DIM model (Luo et al. 2012):

$$\varepsilon_l\rho_l^*\frac{\partial\Omega_{Al}}{\partial t}+\rho_l^*\boldsymbol{V}_l\cdot\nabla\Omega_{Al}=\nabla\cdot\left(\varepsilon_l\rho_l^*\boldsymbol{D}_{Al}^*.\nabla\Omega_{Al}\right)+\ \rho_l^*\alpha\left(1-\Omega_{Al}\right)\left(\omega_{eq}-\Omega_{Al}\right) \tag{10}$$

$$\frac{\partial\varepsilon_l\rho_l^*}{\partial t}+\nabla\cdot\left(\rho_l^*\boldsymbol{V}_l\right)=\rho_l^*\alpha\left(\omega_{eq}-\Omega_{Al}\right) \tag{11}$$

$$-\rho_s\frac{\partial\varepsilon_s}{\partial t}=\rho_s\frac{\partial\varepsilon_l}{\partial t}=\rho_\beta^*\alpha\left(\omega_{eq}-\Omega_{Al}\right) \tag{12}$$

where, ρ_l^* is the effective density, $\alpha=\alpha(\varepsilon_l)$ the mass exchange parameter and $\boldsymbol{D}_{Al}^*$ is the macroscopic diffusion/dispersion tensor. Recall that $\varepsilon_l=V_l/V$ is the classical definition of the porosity, $\varepsilon_s=V_s/V$ is the solid volume fraction which can be expressed in term of void ratio *e*, $\varepsilon_s=e/(1+e)$. The value of the macroscopic effective coefficients (value at the Darcy scale) are obtained thanks to the solution of the "closure problems" over a unit cell, whose shape and topology is specific to the considered porous medium as pictured in Fig. 5.

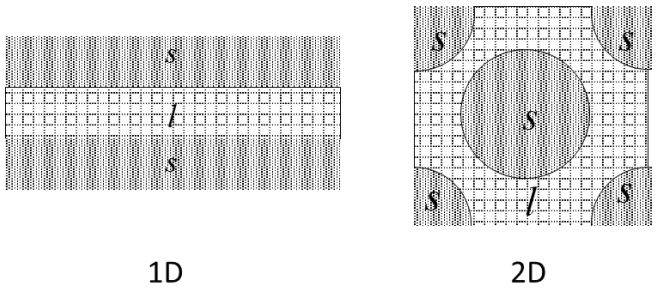

Figure 5. Pictures of unit cells defining the domain of the closure problems.

Their expression according to Luo (Luo et al., 2012) are:

$$\boldsymbol{D}_{Al}^{*} = \boldsymbol{D}_{Al}\left(\boldsymbol{I} + \varepsilon_l^{-1} \frac{1}{V} \int_{A_{ls}} \left(\boldsymbol{n}_{ls} \boldsymbol{b}_l \right) dA \right) - \varepsilon_l^{-1} \left\langle \boldsymbol{b}_l \tilde{\boldsymbol{v}}_l \right\rangle \tag{13}$$

$$\alpha = \frac{1}{V} \int_{A_{ls}} \frac{\rho_l}{\left(1-\omega_{eq}\right)} D_{Al} \left(\boldsymbol{n}_{ls} \cdot \nabla s_\beta \right) dA \tag{14}$$

$$\rho_l^{*} = \frac{1}{\varepsilon_l \ \Omega_{Al}} \left\langle \rho_l \, \omega_{Al} \right\rangle \tag{15}$$

$\boldsymbol{b}_l$ and s_l two variables, solutions of the boundary value closure problems.

It is noteworthy that these physical properties, $\boldsymbol{D}_{Al}^{*}$, ρ_l^{*} and α at the macroscopic scale are by no means not phenomenological nor measured experimentally. The macroscopic properties are based on physical properties established at the pore scale.

In the case of DIM the mass exchange coefficient expression $\alpha = \alpha(\varepsilon)$ as a function of porosity is quite arbitrary. In any case $\alpha = \alpha(\varepsilon)$ must fulfill the condition shown in Fig. 6.

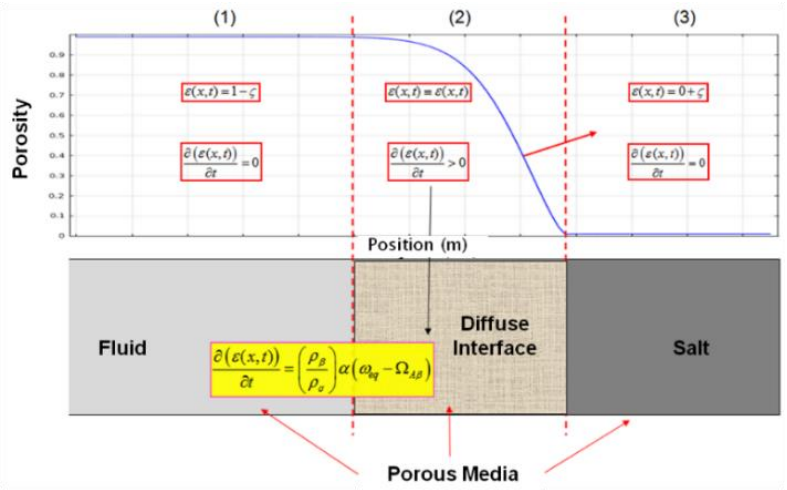

Figure 6. Porosity evolution and rate condition in the whole porous media including diffuse interface

At this scale, the fluid velocity can be described either by the classical Darcy model or the Darcy-Brinkman version (Brinkman, 1947)

$$\frac{\mu_l\left(\Omega_{Al}\right)}{\varepsilon_l} \Delta \boldsymbol{V}_l - \left(\nabla P_l - \rho_l^{*} \boldsymbol{g} \right) - \mu_l\left(\Omega_{Al}\right) \left(\boldsymbol{K}\left(\varepsilon_l\right) \right)^{-1} \cdot \boldsymbol{V}_l = 0 \tag{16}$$

with $\boldsymbol{K}(\varepsilon_l)$ the permeability tensor. This model will tend to Stokes equation when $\boldsymbol{K}(\varepsilon_l)$ is very large and lead to Darcy's model when $\boldsymbol{K}(\varepsilon_l)$ is very small. Note that the inertial terms are supposed negligible.

In the following section we illustrate the use of the methodology in the analyses of some dissolution examples.

2.3. Modelling of direct leaching process in salt mass

This section discusses the application of the proposed approach described in the above section. The first application consists in the modeling of a direct leaching test performed in a salt mass. We compare the results of the modeling to the experimental measures. The goal is to illustrate the capacity of the approach to face problems with geometrical singularity and important density impacts resulting from the high salt solubility.

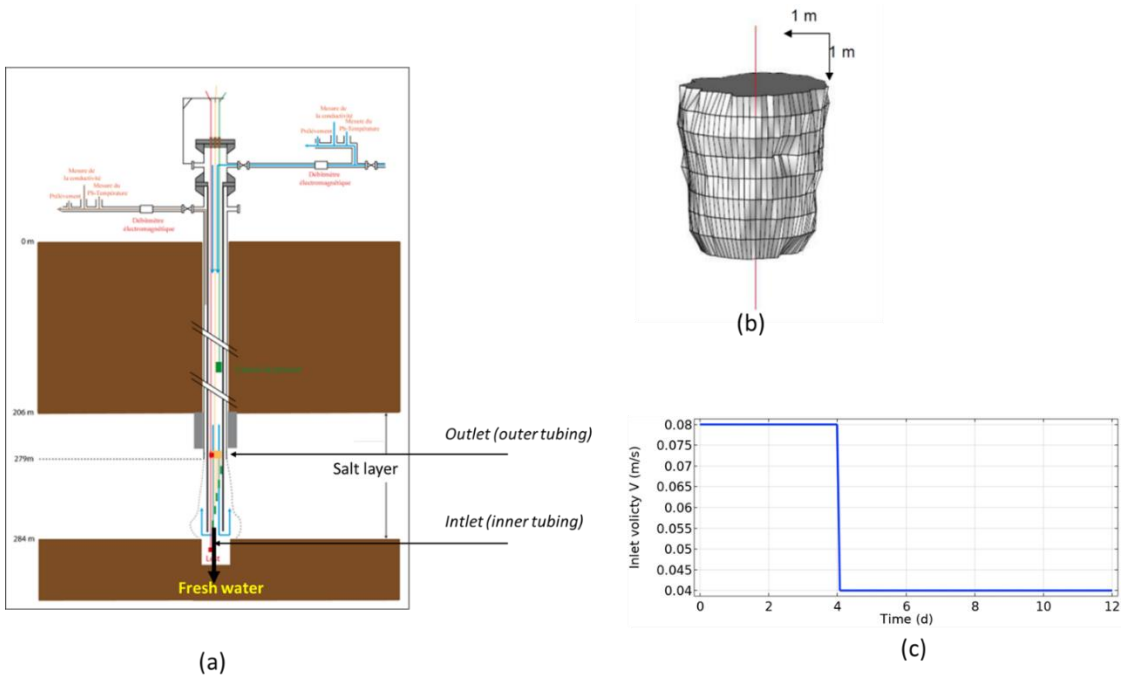

Figure 7. Configuration of the experimental leaching test (a), Resulting dissolution after twelve days of freshwater injection (b) and inlet velocity history (c) (after Charmoille et al. 2012)

The principles of the experimental in-situ test are as follows. Two concentric tubes are driven into the ground to a depth of 280 m (Fig. 7a). Through the central tube, water is injected continuously during several days. The injection by the central tube is known as the *direct leaching method*. The injection history is given in terms of velocity in Fig. 7c and is of 3 m^3/h for 4 days and 1.5 m^3/h for 8 days. A sonar test of the dissolution void was carried out and it was deduced the final form obtained which was quasi-cylindrical as illustrated in Fig. 7b.

In the numerical modelling of this direct leaching process we first suppose that the problem is axisymmetric. Proper initial and boundary conditions describing this problem are applied in the numerical model solved using finite element method. The liquid (brine) density ρ_l (kg/m^3) has the following expression

$$\rho_l(t,\boldsymbol{x}) = 1000 + 738.5\ \omega_{Al}(t,\boldsymbol{x}) \tag{17}$$

with $\omega_{Al}(t,\boldsymbol{x})$ the mass fraction of species A at time t and point $\boldsymbol{x}$. The mass fraction at equilibrium ω_{eq} is equal to 0.27. The salt density ρ_s is equal to 2165 kg/m^3. The liquid dynamic viscosity is supposed constant and equal to 10^{-3} Pa s and the diffusivity is equal to 1.3×10^{-9} m^2/s. The permeability of the salt rock is equal to 10^{-20} m^2. The numerical results of this experimental test are shown hereafter. Fig. 9 shows at different times or value of the porosity inside the domain in the axisymmetric plane. We observe on this figure the development of a near-cylindrical cavity, a shape that is maintained over time. The gradient of color between the "fluid" part (red) and the "solid part" (blue) indicates the existence of the diffuse interface of a finite width.

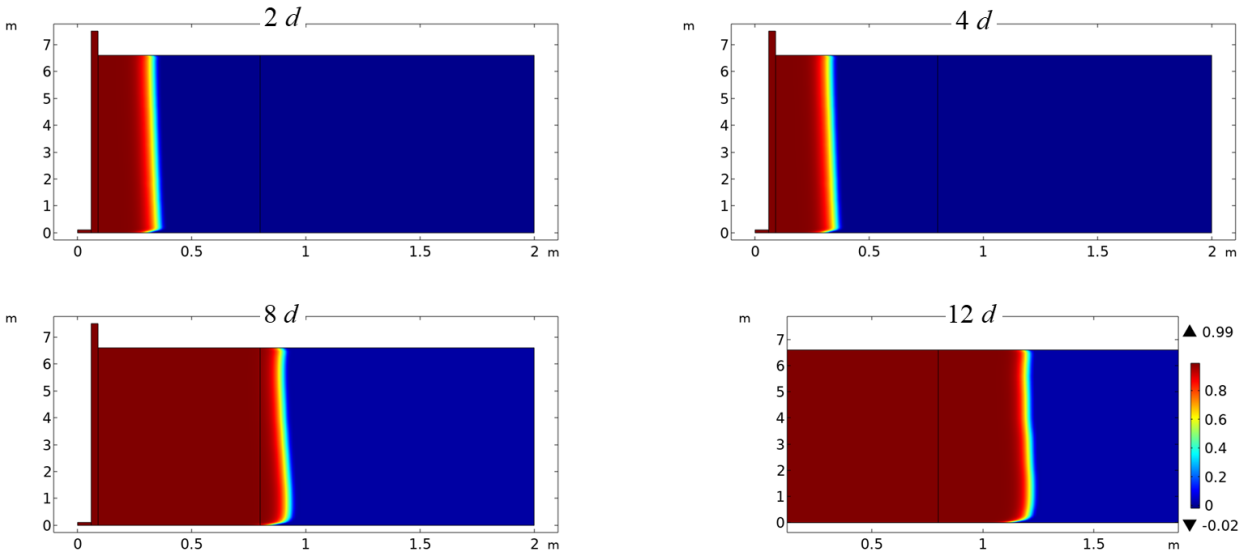

Figure 8. Isovalue of the porosity after 2, 4, 8, and 12 days. Void for unity.

The computed dissolved volumes are around 12 m^3 after 4 days and 38 m^3 after 12 days. The experimental evaluation of the cavity volume deduced from the outlet fluid composition analysis, are around 11 m^3 and 40 m^3, respectively. This demonstrates the accuracy of the numerical model.

The flowlines (Fig. 9) shows at different times or cavity volume, the natural convection effect linked to concentration (mass fraction) gradients due to the strong solubility of salt.

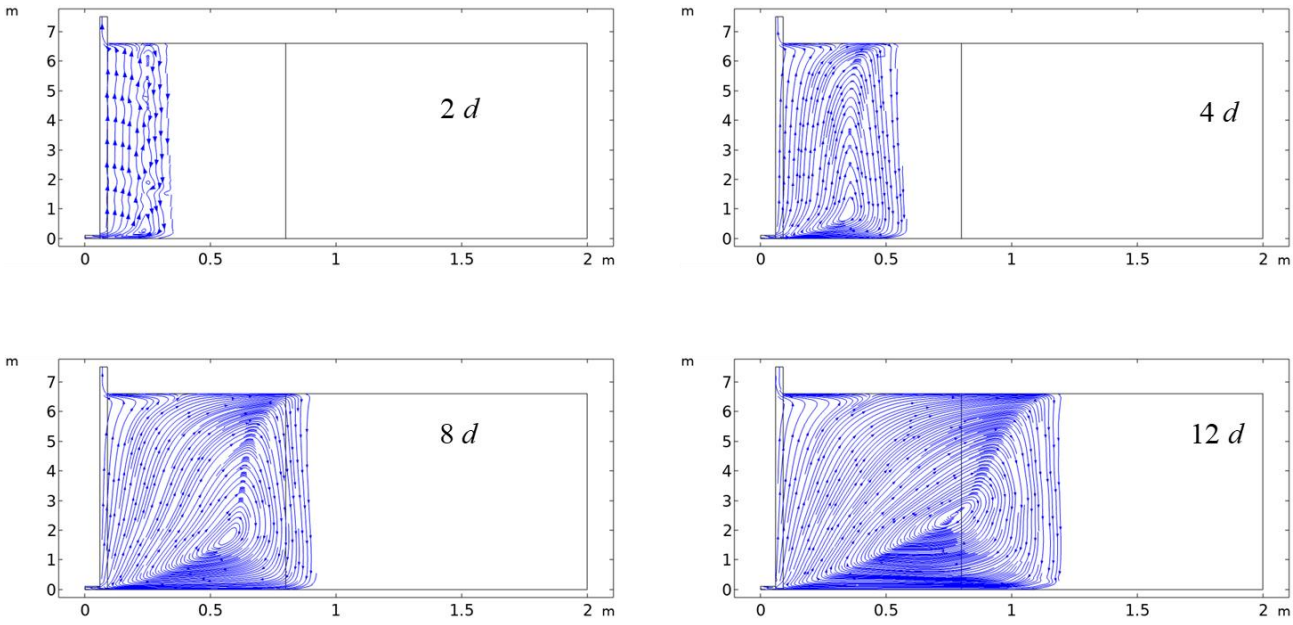

Figure 9. Streamlines and fluid vectors field after 2, 4, 8, and 12 days.

On figure 10 we have represented at six instants the position of the liquid/salt interface. In this point tracking we have considered the interface situated at mid-height (segment AA). It is noteworthy that the interface is not sharp but has a finite thickness.

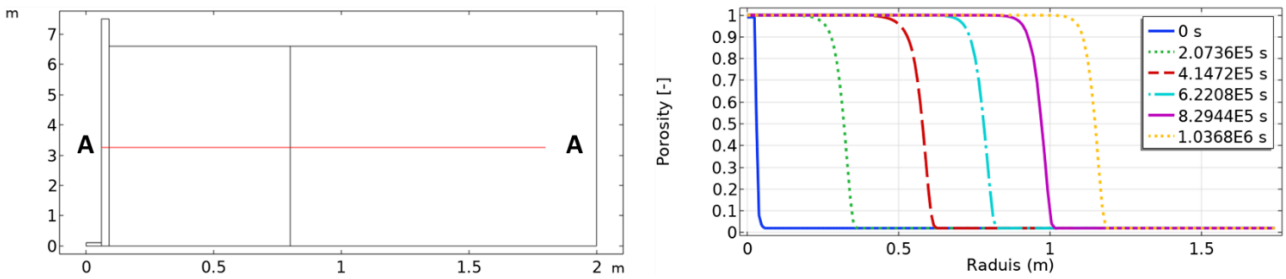

Figure 10. Example of diffuse interface shape and location along the line AA.

With the same boundary conditions as above, we consider now instead of salt a gypsum domain and the associated parameters (Guo et al. 2016). In these computations the liquid density is kept constant (very small solubility) and equal to 1000 kg/m^3. Fig. 11 shows the cavity at different times (1, 5, 10, 30 years). We observe the very slow dissolution rate (small cavity after a long time) for gypsum material and the different cavity shapes compared to those obtained with salt.

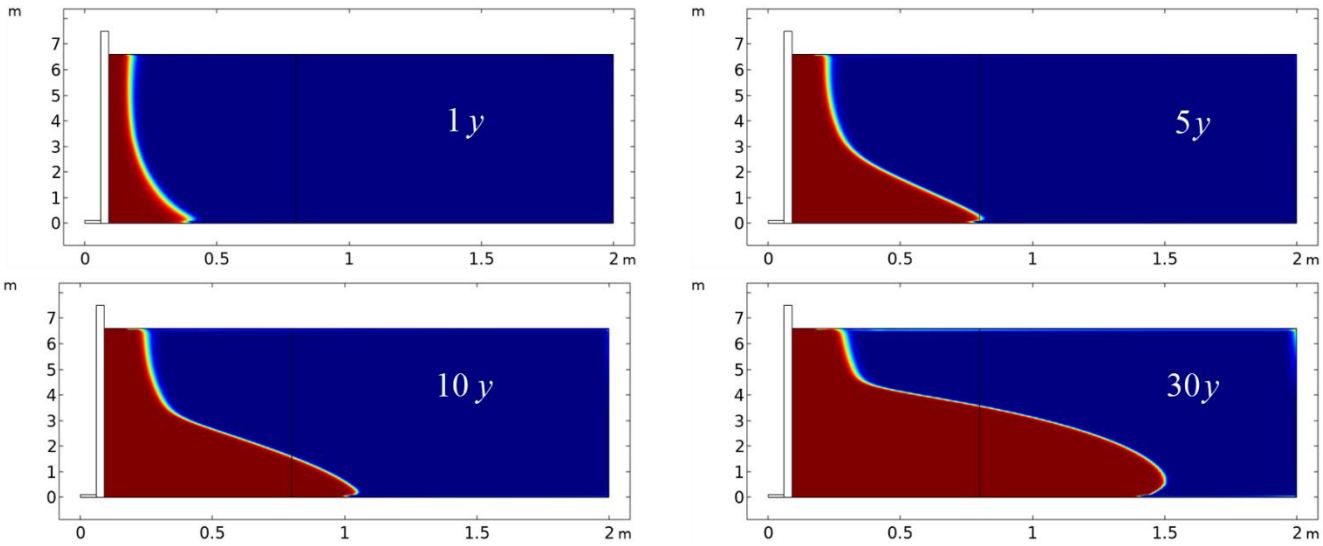

Figure 11. Shave of the cavity in gypsum after 1, 5, 10, and 30 years (Void is red).

In this case there is no convection induced by liquid density gradient. We can note that the value of solubility is not the only parameter controlling the interface recession rate. At a point of the interface, the rate of dissolution (recession rate) depends on the concentration gradient, the fluid velocity, among others. Fig. 12 below illustrates these remarks. Let us denote $\bar{\tau}(\underline{x},t)$ as the value of the recession rate-rate of dissolution (unit: mass per unit surface per time) at the point ($\underline{x}$) of the fluid-solid interface and at time t. Its expression is

$$\bar{\tau}(\underline{x},t) = \rho_s \left(\int_0^L \frac{d}{dt} \varepsilon(x,t)\, \mathrm{d}x \right) \tag{17}$$

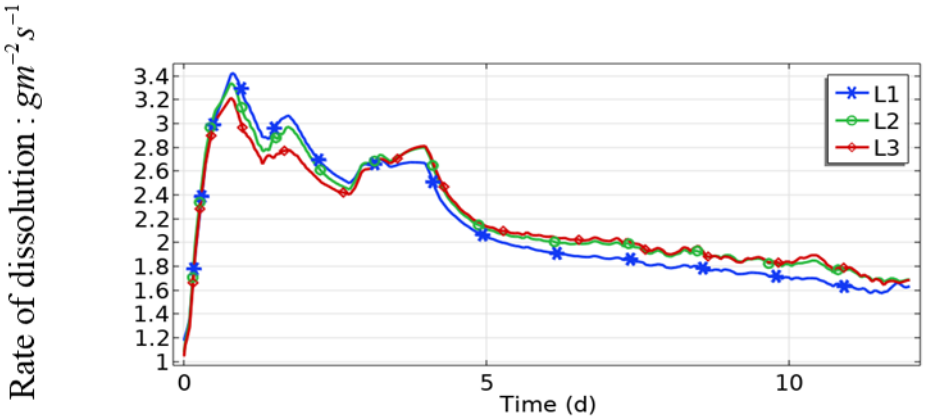

Figure. 12. Time evolution of the recession rate along three lines located in salt layer (Bottom-L1,Middle-L2, ,Top-L3). Case of direct leaching process in salt mass (Figure 7).

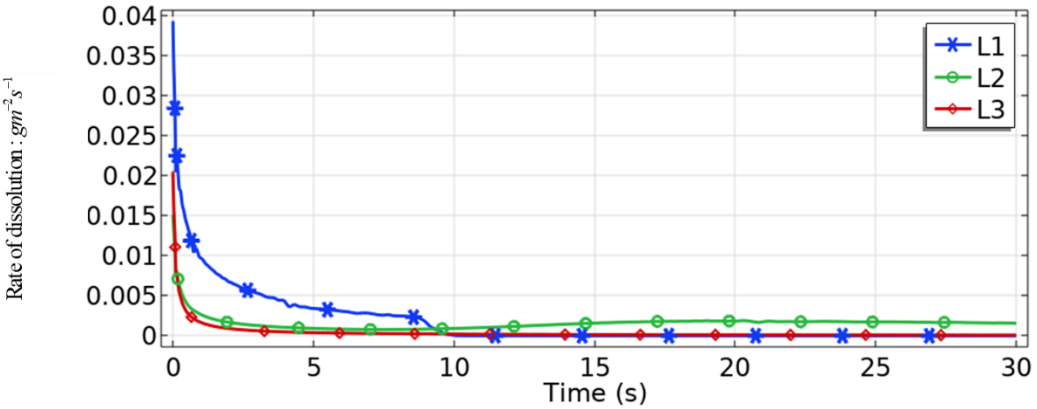

Figure. 13. Time evolution of the recession rate along three lines located in gypsum layer (Bottom-L1,Middle-L2, ,Top-L3). Case of direct leaching process in salt mass (Figure 7).

We can observe that the recession rate is far from being constant in time either for salt or for gypsum. So, this does not make sense to use a unique and constant value for the dissolution rate, as often done in engineering practice, since it evolves according to the hydrodynamic conditions and the chemical composition of the fluid. We also observe the significant difference between the dissolution rate of salt and those of gypsum.

The proposed approach can be improved and extended to problems with more complex chemistry involving multiple components for instance, by also taking into account the presence of non-soluble particles within the porous matrix, etc. The accuracy of the method can be increased, however although these aspects are of undeniable scientific interest, we are often restricted, in-situ, by the lack of information and data. At this time, the approach is sufficiently accurate for the geoengineering problems that we are dealing with and has been successfully applied in other cases.

3. Applications of dissolution modelling in geotechnical fields

In the following 2D and 3D examples, we consider several coupled problems involving gypsum. The first case corresponds to dissolution under an elastoplastic soil. A gypsum rock

is located below and in the vicinity of a dyke (soil slope). In many countries there exists gypsum layer very close to the surface (Toulemont, 1981, 1987).

The gypsum domain is contained in a porous layer and is located between two layers of marl for instance. The flow is induced by a natural hydraulic gradient. We will analyze the time evolution of the plasticity in the soil during the dissolution process.

The second case is about the dissolution of the bottom part of cubic elastoplastic gypsum pillar with geometric singularities (corners) at all edges. We will analyze also the time evolution of the plasticity affecting the pillar during the dissolution process.

These two simple examples show the predictive nature of the proposed approach.

3.1 Gypsum lens in the vicinity of a dyke

The starting point for this numerical modelling is the in-situ observations made in the Val d'Orléans (France). Numerous levees exhibited sinkholes that were developed at different locations (Fig. 14). The process leading to the formation of sinkholes or the failure of the slope is linked to the existence of a void at the base, which was created by dissolution. To the existence of the void is added a phenomenon of soil internal erosion (suffusion). This process involves the removal of fine particles and modifies the mechanical features of the soil. After some time of internal erosion, the instability occurs (Yang et al. 2020). The goal of our simulation is to quantify the time needed to create a critical cavity length.

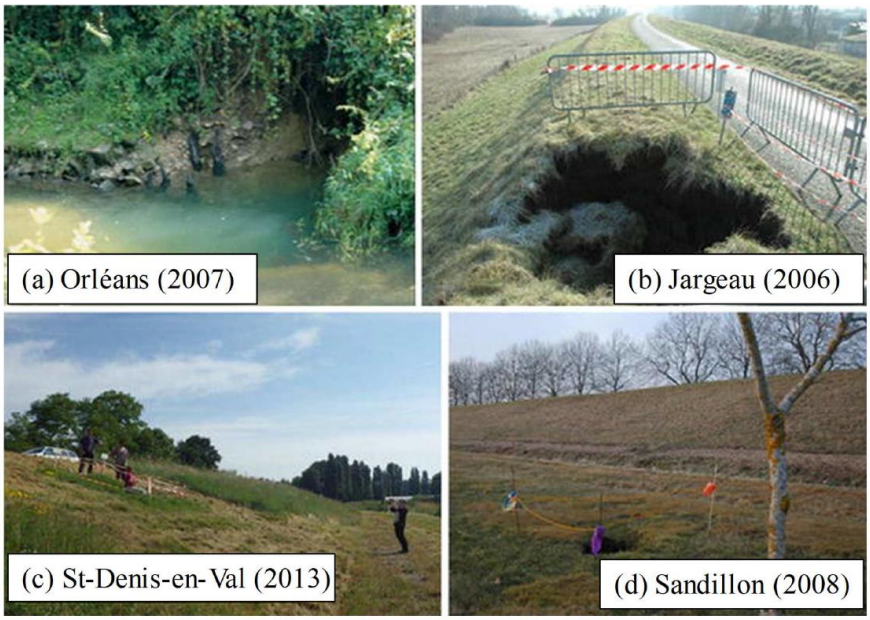

Figure 14. Real case induced by karst existence and the geotechnical failure of some dikes in Val d'Orléans (France). The failure affects the toe (a), the head (b), the slope face (c) and (d) behind the dike (after Gombert et al.,2015)

The problem treated in this section is related to the stability of a dike in the presence of a soluble saturated gypsum domain which dissolves continuously in time. This dissolution is caused and sustained by constant flow of freshwater (Fig. 15).

The gypsum layer (G) of 4 m thickness and 20 m length (Fig. 15) is located just below an overburden (L1, L2) of (sandy-silty) soil. The gypsum domain (G) is situated in a porous medium (L3) saturated with water. Pure water thus flows at the inlet with a continuous velocity V of 2.5×10^{-7} m/s. It is supposed that the inlet concentration is zero (freshwater). A null flow condition is imposed on the lower and upper sides of the porous layer (L3) that contains the soluble part. The mechanical parameters of the soil and of the layers below the soil layer as well as those related to the dissolution are given in Table 1.

Table 1 : Mechanical and dissolution parameters of the model

	E (MPa)	ν (-)	φ (°)	C (kPa)	K (m^2)	μ (Pa s)	ρ (kg/m^3)	α (-)
Layer L1	95	0.35	30	17	-	-	2000	-
Layer L2	190	0.35	35	37	-	-		-
Layer L3	35000	0.35	-	-	10^{-16}	10^{-3}	2300	$5\ 10^{-6}$
Layer G	35000	0.3	-	-	10^{-14}	10^{-3}	2300	$5\ 10^{-6}$

The normal displacement is imposed at all boundaries of the domain. The initial stress state is computed with gravity as the only loading. A very fine elastic (membrane) and highly deformable layer is located at the base of layer L2. The mechanical properties are such that they make possible to dissolve a significant width without numerical instability. Indeed, when the cavity is created, the mechanisms linked to the effective collapse of the ground bell are not described in our approach. The resolution of mechanical and dissolution problems is solved using also finite element method.

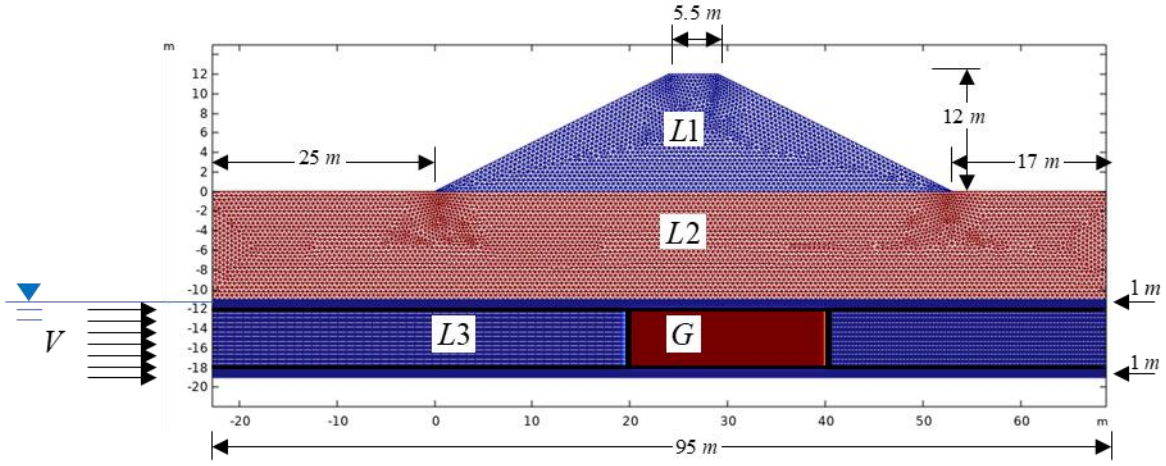

Figure 15. Model meshed of a dike (L1). The gypsum lens (G) is located below and in the vicinity of a dyke.

In this example we used a simple associated elastic perfectly plastic Mohr-Coulomb model and the computation are performed in 2D plane strain condition. In Fig. 16 we show the growth of the dissolution-induced cavity and its impacts in terms of soil layer plasticity (effective plastic strain $\bar{\varepsilon}^{ep} = \int \sqrt{\frac{2}{3}\left(d\varepsilon_{ij}^{p}\ d\varepsilon_{ij}^{p}\right)}$) at 3 times (40, 92 and 106 y), where we observe the extension and the distribution as a function of the intensity of the lens dissolution.

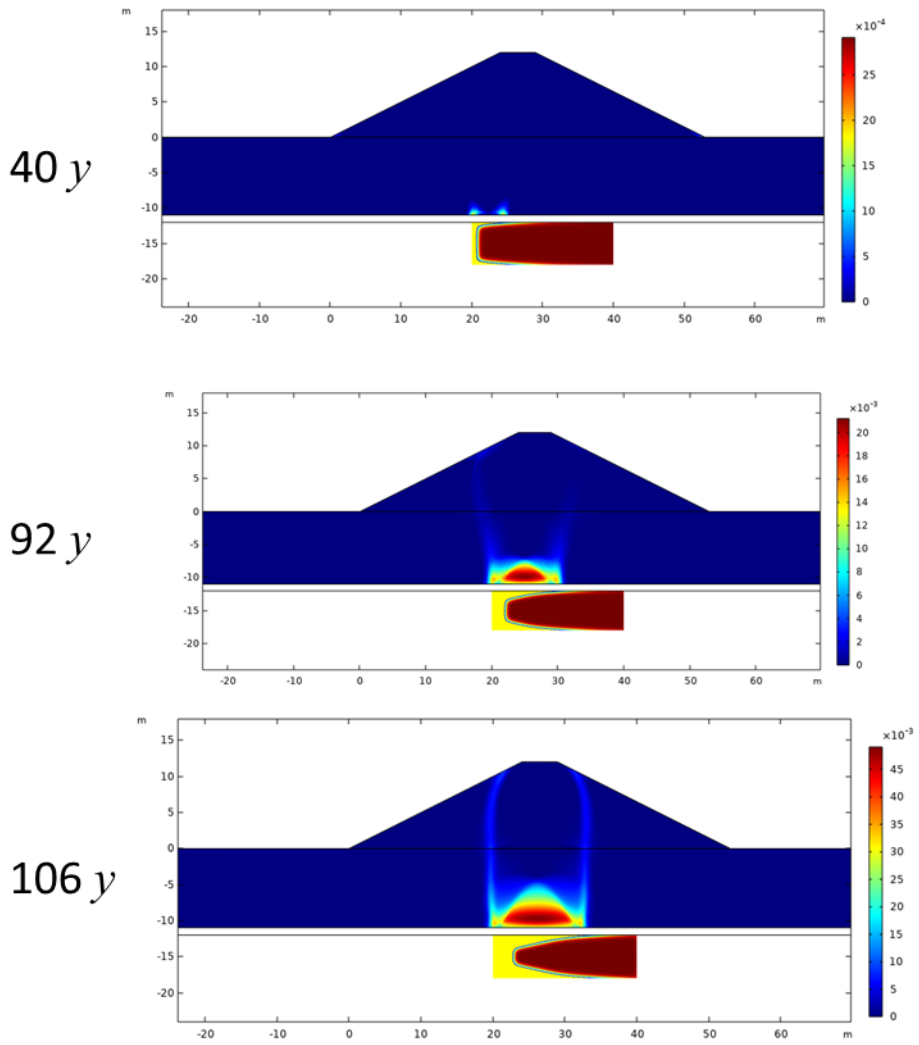

Figure 16 Growth of the dissolution-induced cavity and the impacts in terms of soil layer plasticity at 3 instants 40, 92 and 106 years. (In yellow, the dissolved gypsum cavity)

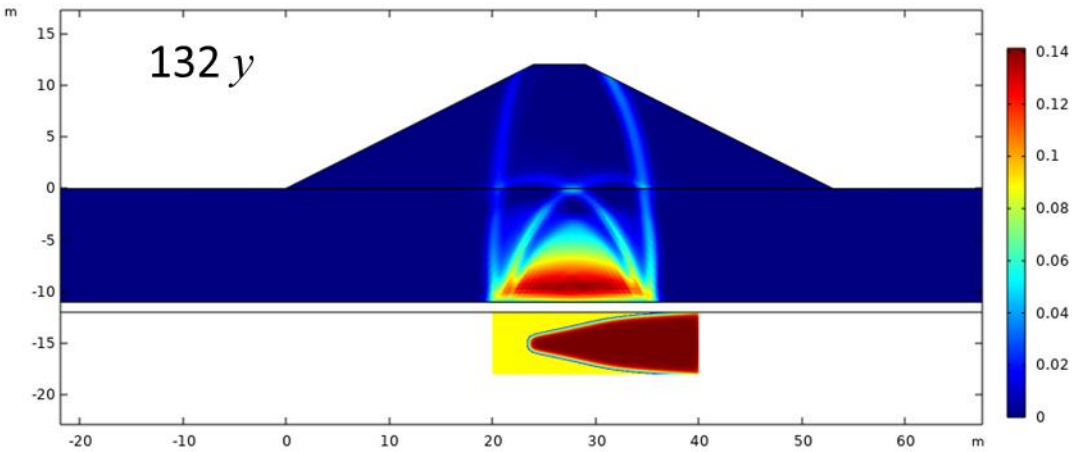

Figure 17 Growth of the dissolution-induced cavity and the impacts in terms of soil layer plasticity at after 132 years. (In yellow, the dissolved gypsum cavity)

As expected, when dissolution progress, plasticity develops in the soil recovery (Figs 16 and 17). The method provides interesting information, especially on the reduction of the stability reserve as a function of time. The knowledge of this evolution can be used for mitigation procedures and to prevent possible damages.

The maximum extension of the cavern is about 16 m at the floor and the roof of the gypsum layer after 132 years. As the dissolution rate is naturally dependent on the boundary conditions, a greater flow velocity will significantly reduce this time. A rainwater inflow, for instance, can naturally create additional preferential dissolution locations within the gypsum rocks. A thorough approach that integrates the history and periodicity of soil surface rainfall is feasible with no particular problems.

We observe that dissolution of the gypsum layer occurs on the boundaries which are gradually reduced. The dissolution does not occur strictly inside the porous gypsum layer because solubility is so low that the equilibrium concentration is reached very fast.

The stability of the soil structure in our analysis is carried out with respect to a criterion of plasticity or the loss of convergence of the Newton-Raphson algorithm. More relevant criteria such as the positivity of the second order work (Hill 1958, Prunier et al. 2009) could be used to analyze the stability.

3.3 Elastoplastic gypsum pillar dissolved at its base

In the Parisian region (France), the gypsum layers are very superficial. The thin overburden is not particularly resistant and is highly sensitive to the existence of caverns (Toulemont, 1987). A further issue relates to the flooding (partial or total) of gypsum mines. In certain mines, stability is provided by pillars which are left in place (Fig. 18). Their design is usually safe to consider many uncertainties. However, gypsum is a soluble substance and is therefore very sensitive to water. The influx of water in a continuous or periodical manner over the long period questions the effectiveness of the stability guarantee. In the short or long period of time, according to the hydraulics conditions, the pillars will lose their strength due to the dissolution and the stability of the structure will be threatened.

Figure 18. Photo of pillar in the abandoned quarry with a thin layer of water at its base (by courtesy of Watelet JM, INERIS)

Table 2 : Mechanical and dissolution parameters of the model

	E (MPa)	ν (-)	φ (°)	C (MPa)	K (m^2)	μ (Pa s)	ρ (kg/m^3)	α (-)
Layer L1	350	0.3	-	-	-	-	2300	-
Layer L2	35	0.3	-	-	-	-	2300	-
Pilar P	35	0.3	40	4	$1\ 10^{-14}$	10^{-3}	2300	$1\ 10^{-5}$
"Water"	1	0.3	-	-	$1\ 10^{-14}$	10^{-3}	2300	$1\ 10^{-5}$

The problem of flooded mines is approached from the standpoint of the instability of a gypsum pillar that is affected by dissolution at its base by a thin layer of water. The gypsum pillar is cubic with sides of 5 m (Figs. 20 and 21). A steady flow of fresh water of no concentration in gypsum is applied upstream. Its velocity is $\boldsymbol{V}$ is equal to 5×10^{-6} m/s. The width of the water domain is 0.30 m. The thin layer of water affects only the base of the pillar. Previous works were performed on cylindrically shaped pillar totally affected by water flooding. An example of state of failure is depicted in Fig. 19, the plasticity after 20 years of cylindrical pillar subjected to continuous water flow (fluid velocity 10^{-6} m/s). The pillar is integrally submerged, and the dissolution affects all its height (Laouafa et al. 2021).

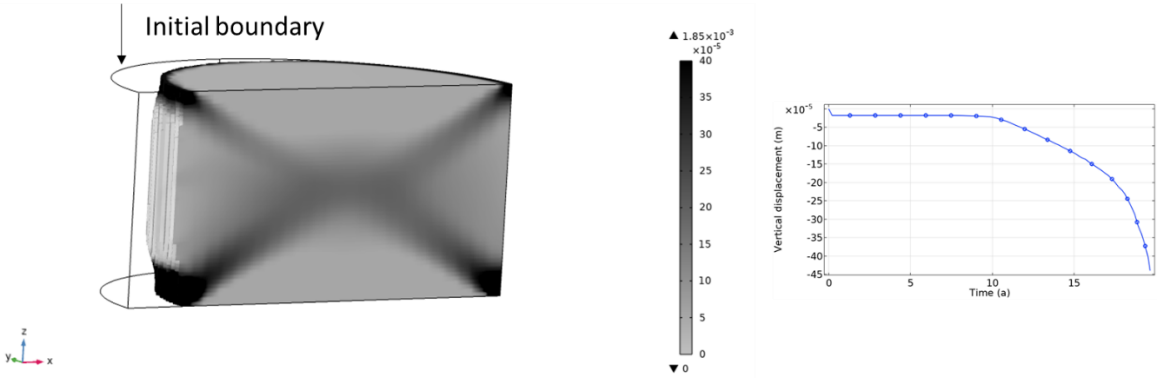

Figure 19. Final shape and plasticity in the pillar before failure and history of the vertical displacement vs time of a point located on the top of the pillar (Laouafa et al. 2021).

In the example below, the water dissolves the base of the cubic pillar, and computations are performed in order to analyze the plasticity or damage distribution evolving during dissolution. A dead load *P* equal to 450 kPa is applied on the top of the surface. The transport mechanical parameters are given in table 2.

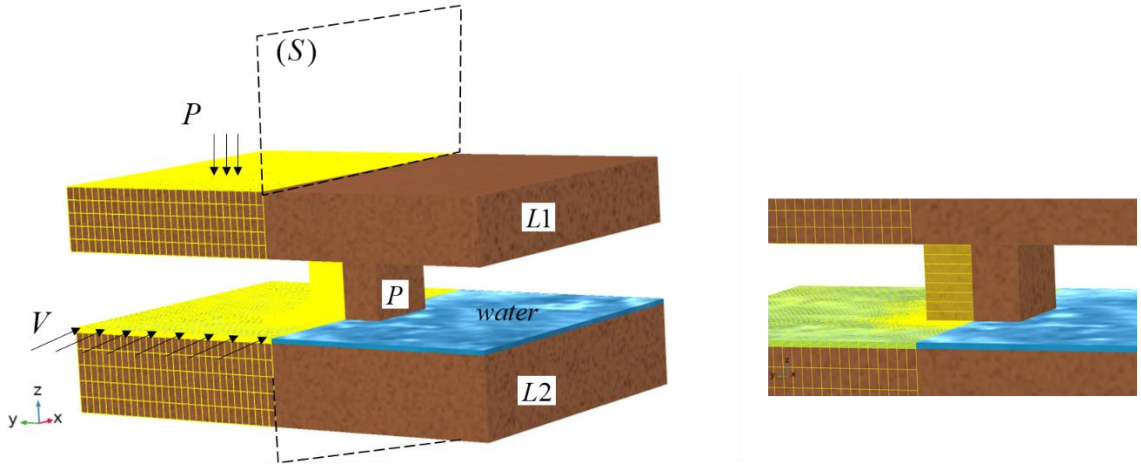

Figure 20. Domain of the model and mechanical loading (P) and flow velocity (V). (S) is a symmetry plane. Only half domain is considered for the analysis

The due to symmetries (geometry, physics) the model used in our computation is shown in Fig 21.

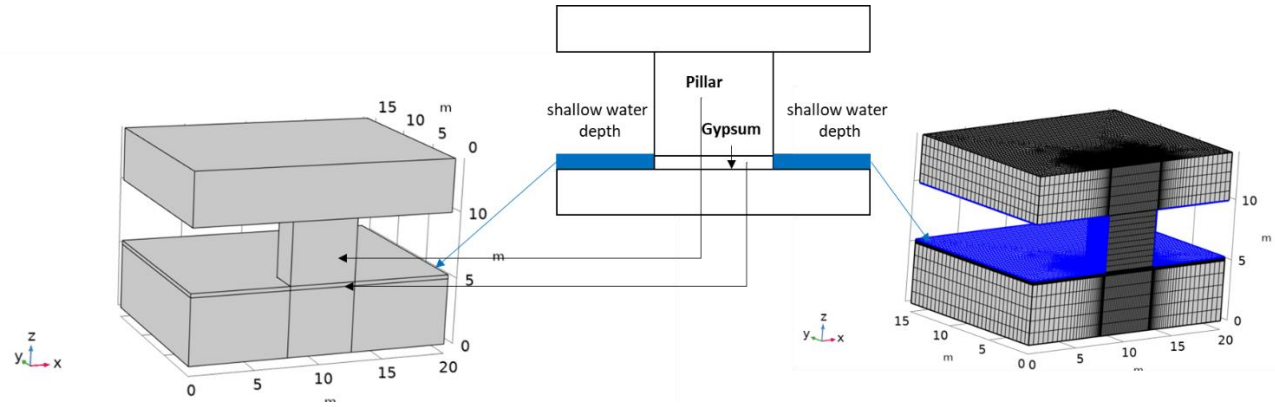

Figure 21. ½ Model (left) and mesh (right) considered in computations.

Fig. 22 shows the development of the porosity or in other terms the progress of the dissolution at four instants (5, 20 50 and 100 years). This is a bottom view of the gypsum layer. We observe a progressive loss of material and therefore of the support of the pillar with time. The symmetry (with respect to the vertical) is preserved owing to the initial conditions. The dissolution is more severe upstream than downstream.

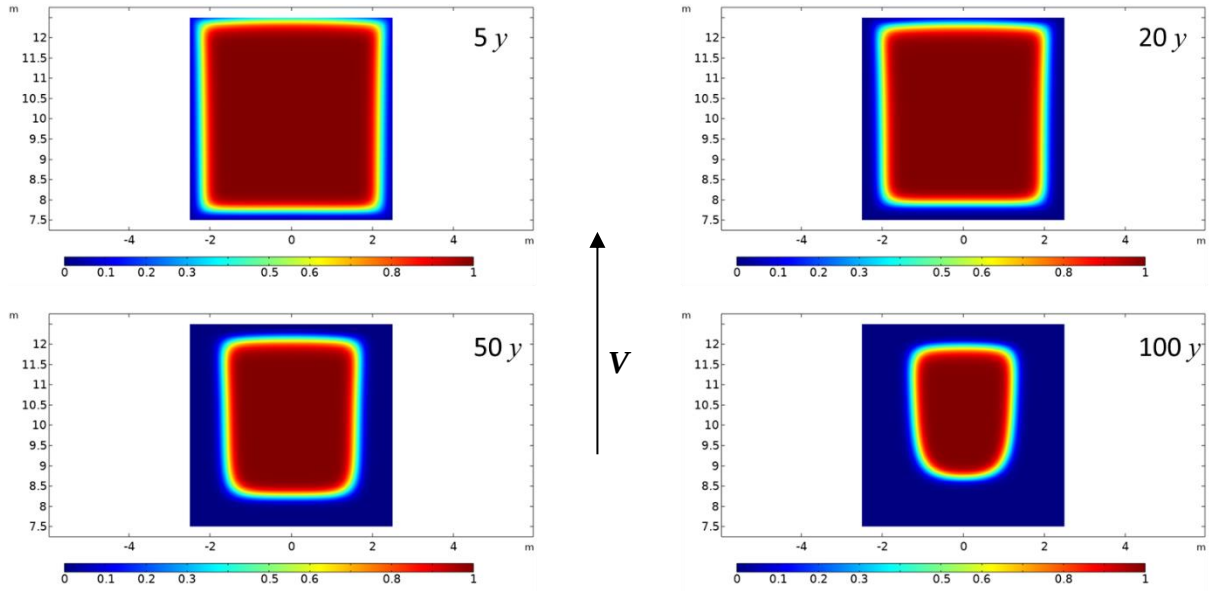

Figure 22. Bottom view of the dissolved gypsum domain after 5, 20, 50 and 100 years. (1 is solid gypsum, 0 is liquid).

Fig. 23 show a 3D view of the gypsum shape lens after 100 years.

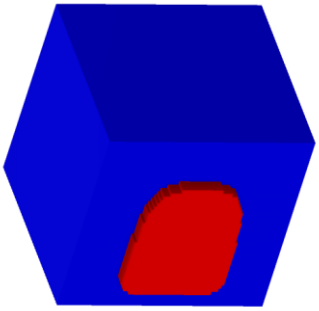

Figure 23. 3D shape (bottom view) of the dissolved gypsum domain after 100 years until numerical convergence.

In figure 24 we can visualize the variation in space and for various times of the concentration of the chemical species. This description is carried out at mid thickness of the water layer. Four instants are shown: 5, 20, 50 and 100 years. The normalized concentration field evolves both in intensity and in extension as dissolution progresses.

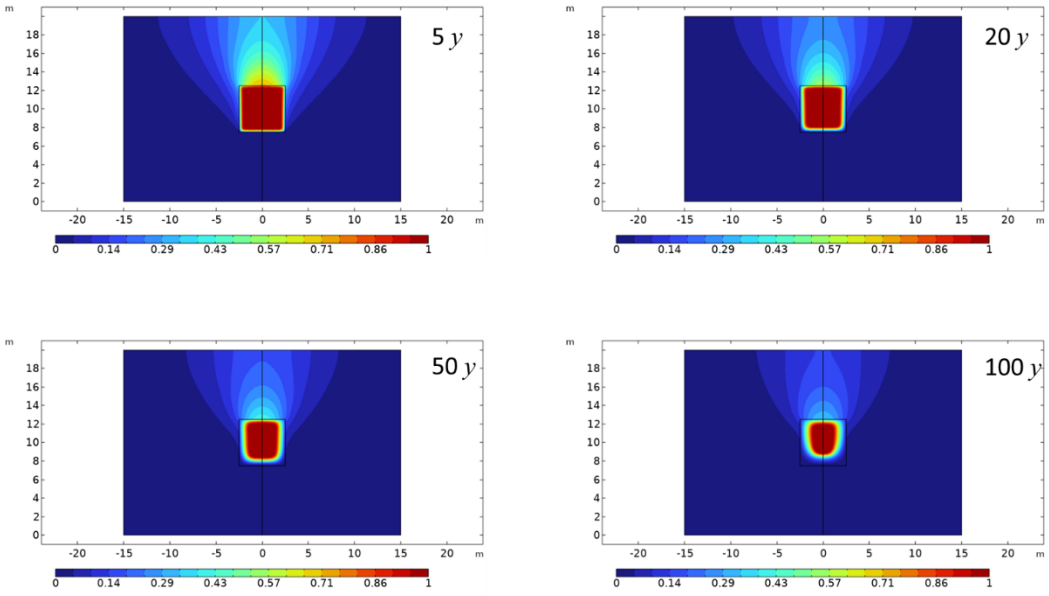

Figure 24. Variation in space and for various times (5, 20, 50 and 100 y) of the concentration of the chemical species. Description carried out at mid thickness of the water layer.

Figs. 25 shows the evolution of the effective plastic strain with the progression of dissolution. The elastoplastic pillar and the geometric configuration of the gypsum lens at different times are shown in this figure.

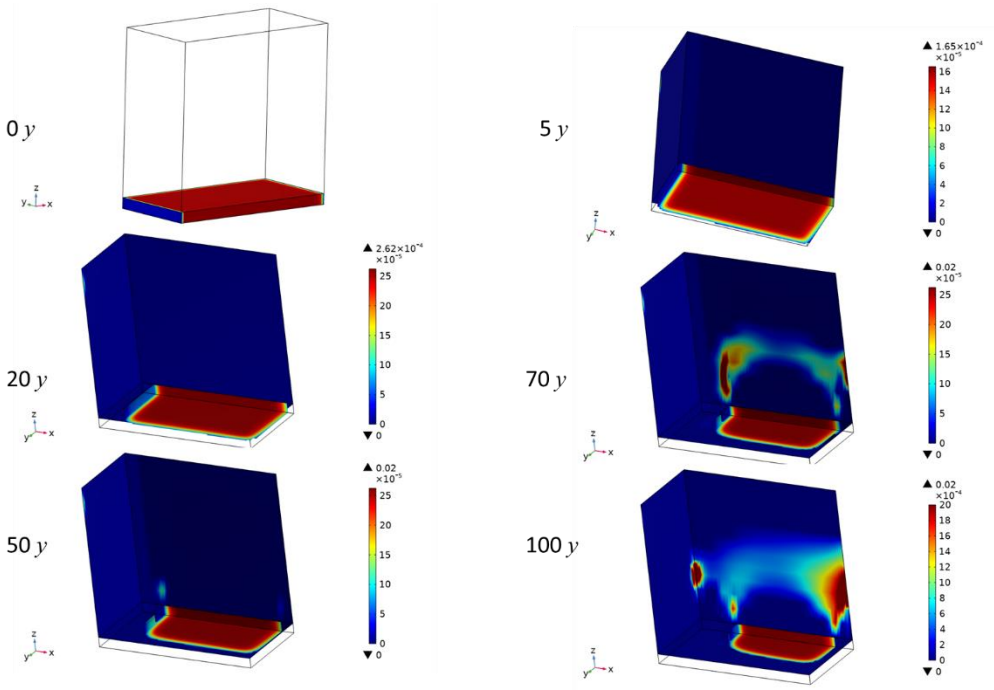

Figure 25. Time evolution of 3D spatial distribution of effective plastic strain in ½ pillar at different times (0, 5, 20, 50, 70 and 100 years).

It is noticed that dissolution of the base of the pillar leads to a concentration of stress at the boundaries of the area concerned by the dissolution. The more pronounced the dissolution is, the more the stress on the pillar increases in intensity and expands into the pillar. The distribution of plasticity and failure that can be expected is not classical.

This is illustrated in Fig. 26 where we have only represented the plastic zones in the interior of the pillar. It is noteworthy that the effect of a thin layer of water, as compared to a total flooding, is not so common.

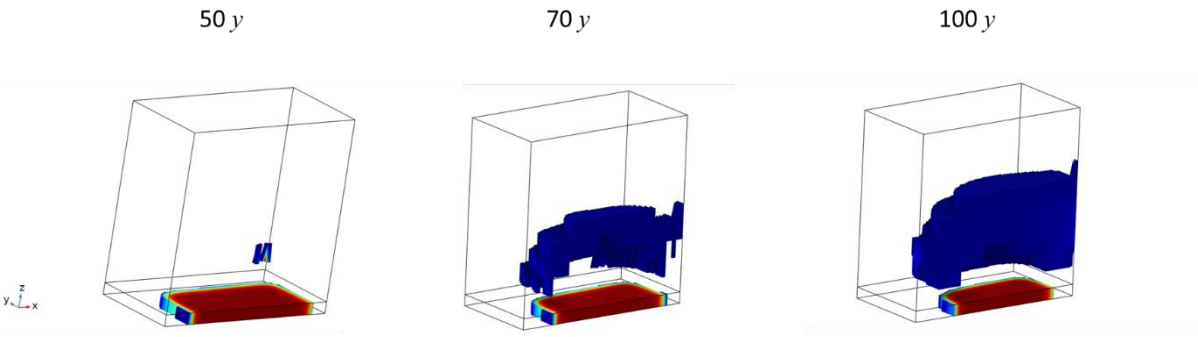

Figure 26. 3D view of part of pillar affected by plasticity for three times (three states of dissolution)

This is also a simple example regarding the elastoplastic model which is used to describe the behavior of gypsum material. The dissolution approach has no particular limitation on the model complexity to use.

In this case it is worth noting that the edges of the soluble domain constitute geometrical singularities and the DIM method can easily circumvent them thanks to its formulation.

The character of the coupling is also notable. For the same reasons mentioned above, the dissolution does not occur in the gypsum mass but on the periphery.

4. Concluding remarks

We have discussed in this paper the modeling of the dissolution of rock materials and its application in geoengineering problems. We have limited the analysis to a soluble medium that contains two phases, a porous solid phase and a liquid phase. The porous soluble medium is saturated with liquid. After the presentation of the method used to model the dissolution built on the basis of microscopic considerations and upscaling, we have applied this method in geotechnical/geomechanical applications. The issue is of noteworthy importance and the findings are very promising. The question of mid- and long-term mechanical behavior will still arise in the presence of water in the vicinity of the evaporite present in the subsurface. The dissolution leads to a perturbation of the surroundings by the formation of voids, the modification of the morphology of structural elements, etc.

By coupling the method that describes dissolution to the geotechnical method, we explicitly introduce time (although the mechanical behavior is independent of time). It is therefore possible to foresee possible losses of stability, such as sinkholes, landslides, failure of structures, etc.

The developed method can be also used in the framework of underground structures like tunnels, pipelines, structures under buildings, close to railroad tracks, etc. Its contributions will be significant in the occurrence of an event (pipe breakage, leakage, water intrusion, etc.).

A problem with the phenomenon of dissolution is that it is relatively slow (notably for gypsum or limestone) and the consequences are visible in the mid- or long term. Another problem is that in-situ dissolution can be only of natural origin. In such a case, we do not

control all the factors (hydraulics for example). The location of the evaporites at the site scale is an additional difficulty.

In this uncertainty context, the proposed approach can have a meaningful contribution.

The developed approach can be extended by introducing a third phase (gas) and heterogeneities at the microscopic scale. The weak coupling in the mathematical sense can be enhanced by incorporating for example the evolution of the porosity induced by the deformation of the medium and by including it in the formulation of the dissolution problem.

References

Anderson D. M., McFadden G. B. (1998). Diffuse-interface methods in fluid mechanics. *Annu. Rev. Fluid Mech.*, 30: 139–165.

Bachmat, Y. and Bear, J. (1987). On the Concept and Size of a Representative Elementary Volume (Rev). In: Bear, J., Corapcioglu, M.Y. (eds) *Advances in Transport Phenomena in Porous Media*. NATO ASI Series, vol 128.

Bell F. G., Stacey T. R., Genske D. D. (2000). Mining subsidence and its effect on the environment: some differing examples. *Environ. Geol.*, 40(1–2): 135–152

Brinkman H. C. (1947). A calculation of the viscous force exerted by a flowing fluid on a dense swarm of particles. *Appl. Sci. Res.*, 1: 27–34.

Castellanza R., Gerolymatou E., Nova R. (2008). An attempt to predict the failure time of abandoned mine pillars. *Rock Mech. Rock Eng.*, 41: 377-401

Charmoille A., Daupley X., Laouafa F. (2012). *Analyse et modélisation de l'évolution spatio-temporelle des cavités de dissolution*. Report DRS-12-127199-10107A. INERIS

Collins J. B., Levine H. (1985). Diffuse interface model of diffusion-limited crystal growth. *Phys. Rev. B*, 31: 6119–6122.

Cooper A. H. (1988). Subsidence resulting from the dissolution of Permian gypsum in the Ripon area; its relevance to mining and water abstraction. *Geological Society, London, Eng. Geol. Spec. Publ.*, 5: 387-390

Donea J., Giuliani S., Halleux J. P. (1982). An arbitrary Lagrangian-Eulerian finite element method for transient dynamic fluid-structure interactions. *Comput. Method Appl. M.*, 33: 689–723.

J. Feng, H. H. Hu, and D. D. Joseph (1994), Direct simulation of initial value problems for the motion of solid bodies in a Newtonian fluid. 1. Sedimation, *J. Fluid Mech.* **261**, 95

Freeze R. A., Cherry J. A. (1979). *Groundwater*. Prentice-Hall.

Gerolymatou E., Nova. R. (2008). An analysis of chamber filling effects on the remediation of flooded gypsum and anhydrite mines. *Rock Mech. Rock Eng.*, 41, 403–419

Gombert P, Orsat J, Mathon D, Alboresha R, Al Heib M, Deck O. Rôle des effondrements karstiques sur les désordres survenus sur les digues de Loire dans le Val D'Orleans (France). *Bulletin of Engineering Geology and the Environment*. 2015, 74 :125-140.

Guo J., Quintard M., Laouafa F. (2015). Dispersion in porous media with heterogeneous nonlinear reactions. *Transp. Porous Media*, 109: 541–570

Guo J., Laouafa F., Quintard M. (2016). A theoretical and numerical framework for modeling gypsum cavity dissolution. *Int. J. Numer. Anal. Meth. Geomech.*, 40: 1662–1689.

Hill R. A general theory of uniqueness and stability in elastic-plastic solids. *Journal of Mechanics and Physics of Solids* 1958; 5:236–249

Gysel M. (2002). Anhydrite dissolution phenomena: Three case histories of anhydrite karst caused by water tunnel operation. *Rock Mech. Rock Eng.*, 35: 1–21

James A. N., Lupton A. R. R. (1978). Gypsum and anhydrite, in foundations of hydraulic structures. *Geotechnique*, 28: 249-272.

Jeschke A. A., Dreybrodt W. (2002) Dissolution rates of minerals and their relation to surface morphology. *Geochim. Cosmochim. Acta*, 66, 3055– 3062.,

Jeschke A. A., Vosbeck K., Dreybrodt W. (2001). Surface controlled dissolution rates of gypsum in aqueous solutions exhibit nonlinear dissolution kinetics. *Geochim. Cosmochim. Acta*, 65(1): 27–34.

Yang, J., Yin, Z. Y., Laouafa, F., & Hicher, P. Y. (2020). Three-dimensional hydromechanical modeling of internal erosion in dike-on-foundation. *Int. J. Numer. Anal. Meth. Geomech.* 44(8), 1200-1218. https://doi.org/10.1002/nag.3057

Laouafa, F., Guo, J. & Quintard, M. Underground Rock Dissolution and Geomechanical Issues. *Rock Mech Rock Eng*. 54**,** 3423–3445 (2021).

Luo H., Quintard M., Debenest G., Laouafa F. (2012). Properties of a diffuse interface model based on a porous medium theory for solid-liquid dissolution problems. *Comput. Geosci.*, 16(4): 913-932

Luo H., Laouafa F., Debenest G., Quintard M. (2015). Large scale cavity dissolution: From the physical problem to its numerical solution. *Eur. J. Mech. B-Fluid*, 52: 131–146

Luo H., Laouafa F., Guo J., Quintard M. (2014) Numerical modeling of three-phase dissolution of underground cavities using a diffuse interface model. *Int. J. Numer. Anal. Meth. Geomech.*, 38: 1600–1616.

Prunier, F., Laouafa, F., Darve, F. (2009). 3D bifurcation analysis in geomaterials investigation of the second order work criterion. *Eur. J. Environ. Civ. Eng.*, 13(2): 135-147

Quintard M., Whitaker S. (1994). Transport in ordered and disordered porous media 1: The cellular average and the use of weighing functions. *Transp. Porous Media*, 14: 163–177.

Quintard M., Whitaker S. (1994). Convection, dispersion, and interfacial transport of contaminant: Homogeneous porous media. *Adv. Water Resour.*, 17: 221–239.

Quintard M., Whitaker S. (1999). Dissolution of an immobile phase during flow in porous media. *Ind. Eng. Chem. Res*., 38: 833–844.

Toulemont M. (1987). Les risques d'instabilité liés au karst gypseux lutétien de la région parisienne – Prévision en cartographie. *Bull. de liaison P. et Ch.*, 3192:109-116.

Toulemont M. (1981). Evolution actuelle des massifs gypseux par lessivage. Cas des gypses Lutétiens de la région parisienne, France. Bulletin de liaison. *Laboratoire régional des Ponts et Chaussées de l'Est parisien*, France.

Swift G. M., Reddish D. (2002). Stability problems associated with an abandoned ironstone mine. *Bull. Eng. Geol. Env.*, 61: 227–239

Tryggvason, G., Bunner, B., Esmaeeli, A., Juric, D., Al-Rawahi, N., Tauber, W., Han, J., Nas, S., Jan, Y.-J.: A front tracking method for the computations of multiphase flow. *J. Comput. Phys*. 169, 708–759 (2001)

Waltham T., Bell F., Culshaw M. (2005). Sinkholes and subsidence, Karst and Cavernous Rocks in Engineering and Construction. Springer-Verlag.

Whitaker S. (1999). *The Method of Volume Averaging*. Kluwer Academic Publishers.